Mussel-Inspired Polydopamine: A Biocompatible and Ultrastable Coating for Nanoparticles *in Vivo*

Xiangsheng Liu, Jieming Cao, Huan Li, Jianyu Li, Qiao Jin, Kefeng Ren, and Jian Ji*

MOE Key Laboratory of Macromolecular Synthesis and Functionalization, Department of Polymer Science and Engineering, Zhejiang University, Hangzhou, Zhejiang 310027, China

ABSTRACT Bioinspired polydopamine (PDA) has served as a universal coating to nanoparticles (NPs) for various biomedical applications. However, one remaining critical question is whether the PDA shell on NPs is stable *in vivo*. In this study, we modified gold nanoparticles (GNPs) with finely controlled PDA nanolayers to form uniform core/shell nanostructures (GNP@PDA). *In vitro* study showed that the PDA-coated GNPs had low cytotoxicity and could smoothly translocate to cancer cells. Transmission electron microscopy (TEM) analysis demonstrated that the PDA nanoshells were intact within cells after 24 h incubation. Notably, we found the GNP@PDA could partially escape from the endosomes/lysosomes to cytosol and locate close to the nucleus. Furthermore, we observed that the PDA-coated NPs have very different uptake behavior in two important organs of the liver and spleen: GNP@PDA in the liver were mainly uptaken by the Kupffer cells, while the GNP@PDA in the spleen were uptaken by a variety of cells. Importantly, we proved the PDA nanoshells were stable within cells of the liver and spleen for at least six weeks, and GNP@PDA did not show notable histological toxicity to main organs of mice in a long time. These results provided the direct evidence to support that the PDA surface modification can serve as an effective strategy to form ultrastable coatings on NPs *in vivo*, which can improve the intracellular delivery capacity and biocompatibility of NPs for biomedical application.

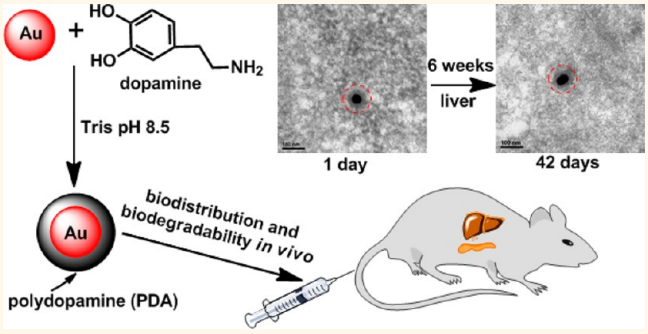

KEYWORDS: nanoparticles · polydopamine (PDA) · cellular uptake · biodistribution · biocompatibility · biostability

Nanoparticle-based nanoscience and biotechnology have shown great promise in biological applications such as drug/gene delivery, biosensing, bioimaging, and photothermal therapy.[1−8] The surface engineering of nanoparticles (NPs) plays an essential role in improving their hydrophilicity, colloidal stability, biocompatibility, and conjugation of bioactive functional groups and hence impacts their interactions with biosystems.[2,9−15] For surface modification, a coating on the NPs with good stability, especially in the complex biological conditions, is strongly desired to realize the surface-mediated interaction and relieve the adverse effect caused by exposing the NP's core. Much effort has been devoted to designing stable surface coatings for NPs, such as polymers with multiple anchoring sites to NPs[11,12,16,17] and silica shell forming a highly cross-linked layer on NPs.[12,18−20]

Recently, Messersmith and co-workers pioneered a single-step formation of robust adherent polydopamine (PDA) films based on mussel-inspired polymerization of dopamine at alkaline pHs on various substrates despite whether the surfaces are hydrophilic or hydrophobic.[21] Moreover, the PDA exhibits latent reactivity toward amine and thiol groups.[21−23] Because of its ease of use combined with its fascinating properties, PDA has attracted considerable interest for various types of applications.[21−32] Notably, the application of PDA to nanomaterials has emerged as a particularly important field. Controllable PDA shells can be formed on the nanoparticles by simply dispersing them in an alkaline dopamine solution and mildly stirring at room temperature.[33−42] The formed PDA shell can serve as molecularly imprinted polymer coatings on nanoparticles for protein recognition.[34,35,39,41]

* Address correspondence to jijian@zju.edu.cn.

Received for review August 7, 2013 and accepted September 8, 2013.

Published online September 08, 2013
10.1021/nn404117j

Additionally, many metal nanoparticles can be formed on the PDA shell *in situ*, which promotes the practically wide applications of these nanocomplexes.[33,35,37,38,43,44] Another important character is that the PDA shell can be further surface functionalized to improve the nanoparticle stability and selective recognition with cells.[45,46] Moreover, PDA-based capsules can be prepared by assembly of PDA thin films onto various particles, followed by removal of the template.[47−50] Cui *et al.* also reported a method of preparing monodisperse PDA capsules with tailoring size, shell thickness, and hydrophobic cargo loading *via* emulsion templating.[51] Westen *et al.* reported on coating liposomes with PDA, which demonstrated their potential as drug delivery vehicle.[52] Melanin-like PDA nanoparticles were prepared by this bioinspired polymerization of dopamine, which had an excellent free-radical-scavenging property.[45]

Because of the bioinspired nature of polydopamine, the bioapplication of PDA has attracted great attention. PDA coatings, which significantly enhanced the adhesion and proliferation of cells, show good biocompatibility and promise for tissue engineering.[53−56] The cytocompatibility of PDA was also demonstrated at the nanoscale. PDA capsules,[47] PDA-coated Fe_3O_4 nanoparticles,[38] and melanin-like PDA nanoparticles[45] were found to have negligible cytotoxicity. Hong *et al.* investigated the biocompatibility of PDA *in vivo*,[36] where they found that one-step PDA coating greatly reduced the inflammatory response to poly-L-lactic acid surfaces and the immunological responses of blood on quantum dots. Meanwhile, PDA has been showing great promise for biomedical applications with fascinating properties. Städler *et al.* demonstrated that the thin film of PDA formed on liposomes or polymersomes, which is beneficial to cell adhesion and proliferation, can be applied to deliver therapeutic agents to cells.[57,58] Cui *et al.* designed stimuli-responsive Dox-loaded PDA capsules as drug delivery carriers, which enhanced the efficacy of eradicating HeLa cancer cells compared to free drug.[50] Most recently, Black *et al.* coated gold nanorods with PDA that facilitated the surface functionalization of gold nanorods with biomolecules, allowing cell targeting and photothermal killing of cancer cells.[46] Interestingly, Liu *et al.* reported that the dopamine-melanin colloidal nanospheres can serve as an efficient near-infrared photothermal therapeutic agent for *in vivo* cancer therapy.[59]

However, as a surface coating, the stability of PDA shell *in vivo* should be considered seriously. It has been known that the PDA will degrade oxidatively with the existence of strong alkaline or hydrogen peroxide.[60] For the *in vivo* case, Bettinger *et al.* showed that the implant melanin thin films seemed to degrade in tissue within up to eight weeks, where the gross erosion of the melanin implant was almost fully completed. This phenomenon could be explained by the rigid properties of melanin implants, which led to fracture of the implant after insertion into the host. The presence of small melanin particulates could have allowed immediate uptake by macrophages and giant cells.[53] However, it is still unanswered whether PDA, especially at the nanoscale, is degradable *in vivo*.[54] Meanwhile, the intracellular degradation of the PDA within cells remains unexplored.

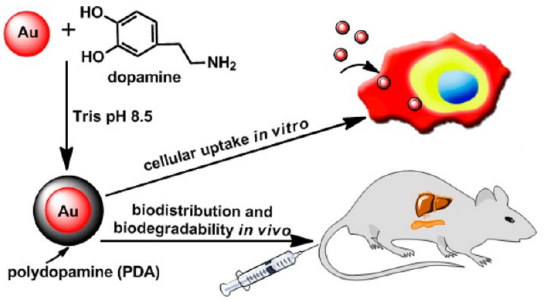

Scheme 1. Preparation of mussel-inspired polydopamine-coated gold nanoparticles (GNP@PDA), *in vitro* cell model, and *in vivo* animal model used in this study (not to scale).

When it comes to the use of PDA for nanomedicine, understanding the interaction between PDA surface and biosystems is very important. In order to better understand the biofate of these mussel-inspired PDA nanoparticles, we designed a core/shell nanostructure (GNP@PDA) with a core of gold nanoparticles (GNPs) and a shell of PDA, and investigated the cellular uptake and biodegradability of PDA *in vitro* and *in vivo* (Scheme 1). Gold nanoparticles have promising applications in fields such as drug delivery and photothermal therapy in oncology due to their unique optical and photothermal properties.[1−3,6,7] Moreover, the design of GNP@PDA with a GNP core in our research has at least two advantages: (1) the uptake of GNP@PDA in cells and tissues can be quantified by detecting the Au content using inductively coupled plasma mass spectrometry (ICP-MS) with high detection sensitivity; and (2) the intracellular localization of GNP@PDA can be clearly observed in cellular compartments by transmission electron microscopy (TEM), as GNPs with high density provide high spatial resolution for TEM analysis.[61] These advantages make the study of GNP@PDA much more accurate and convenient. In this study, we investigated the cytotoxicity and cellular uptake of GNP@PDA with shells of different thicknesses *in vitro*. Furthermore, we studied the blood circulation, biodistribution, and histology of the GNP@PDA in mice. Both *in vitro* and *in vivo*, the biostability of PDA shell was testified after the GNP@PDA being uptaken by cells. The results demonstrate that the PDA modified core/shell NPs have good biocompatibility and can escape lysosome and enter cytosol. Importantly, this work confirms that the PDA nanoshells are stable *in vivo* for a period of at least six weeks.

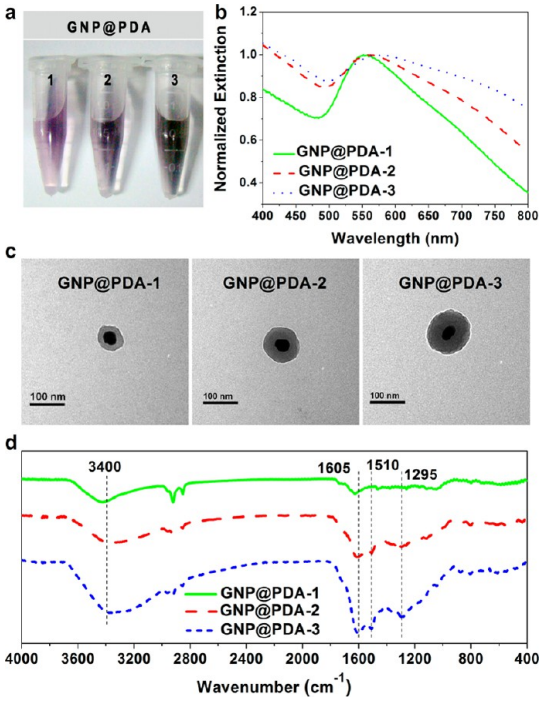

Figure 1. (a) Digital images of gold nanoparticles incubation in dopamine solution with different concentrations of 0.1 (1, GNP@PDA-1), 0.2 (2, GNP@PDA-2), and 0.4 mg/mL (3, GNP@PDA-3) after 1 h reaction. (b) Extinction spectra of purified GNP@PDA as shown in (a). (c) Representative TEM images of GNP@PDA with different shell thickness. (d) FT-IR spectra of purified GNP@PDA as shown in (a).

RESULTS AND DISCUSSION

Synthesis and Characterization of GNP@PDA Core/Shell Nanoparticles. Gold nanoparticles were easily coated with a shell of PDA by dispersing them in a dopamine solution at pH 8.5 and mildly stirring at room temperature for 1 h under air. As shown in Figure 1a, the reaction solution color became black because of the polymerization of dopamine, and the color became darker with increased dopamine concentration from 0.1 to 0.4 mg/mL (Figure S1, Supporting Information, showed the images of plain GNP suspension without PDA and PDA suspension without PDA). In the following discussion, we refer the core/shell particles obtained from the dopamine solution at concentrations of 0.1, 0.2, and 0.4 mg/mL as GNP@PDA-1, GNP@PDA-2, and GNP@PDA-3, respectively. Figure 1b showed the UV−vis spectra of purified GNP@PDA, and all of the PDA-coated GNPs exhibited a characteristic extinction peak around 550 nm due to surface plasmon resonance of 50 nm gold nanoparticles (~535 nm). The slight red-shift for the extinction peak of GNP@PDA was due to the increase of refractive index around GNPs after PDA coating.[1] Besides, GNP@PDA showed obvious absorbance at long wavelength (600−800 nm), which increased when dopamine was used at higher concentration. It could be mainly attributed to the extinction of thicker PDA shell, as the formed PDA at the same condition without GNPs had obvious absorbance at higher wavelengths (Figure S1, Supporting Information). In addition, some GNP@PDA embedded with more than one GNP could also result in an increase of absorbance at higher wavelengths due to coupled surface plasmon in closely located GNPs.[1] In order to minimize the formation of self-polymerized PDA particles, we used the dopamine solution at low concentration, which was lower than 0.5 mg/mL.[33] Few self-polymerized PDA particles existed after purification by centrifugation as confirmed by TEM (Figure S2, Supporting Information). It is expected that the PDA had highly wrapping tendency around nanoparticles due to the preference of nucleation at nanoparticle surfaces,[33,46] supported by a variety of interactions between the PDA and the metal GNP surface, including electron interactions, metal coordination, and electrostatic interactions.[46] Thickness of PDA shell formed on GNP surface changed from ~19 to ~36 nm when the concentration of dopamine increased from 0.1 to 0.4 mg/mL (Figure 1c, Figure S2, Supporting Information, Table 1). It demonstrated that the thickness of PDA shell could be well controlled at the nanometer scale by adjusting the concentration of dopamine. In the FT-IR spectra of GNP@PDA (Figure 1d), absorption bands at 3410 cm^{-1} (stretching vibration of phenolic O−H and N−H), 1605 cm^{-1} (stretching vibration of aromatic ring and bending vibration of N−H), 1510 cm^{-1} (shearing vibration of N−H), and 1295 cm^{-1} (stretching vibration of phenolic C−O), supported the presence of PDA on the GNPs.[26,27] Zeta potential results showed that the all of the PDA-coated GNPs had a negative surface charge, which could be ascribed to the deprotonation of catechol −OH groups on the PDA shells (Table S1, Supporting Information). Table 1 summarizes the physical size and hydrodynamic size of GNP@PDA with different shell thicknesses. The hydrodynamic size of GNP@PDA-3 was much larger than their physical size, indicating that some aggregation happened in the

TABLE 1. GNP@PDA Physicochemical Properties

	GNP core size [nm][a]	physical size [nm][a]	shell thickness [nm][a]	hydrodynamic size [nm] (PDI)[b]
GNP@PDA-1		88.6 ± 6.8	19.0 ± 2.6	101.3 ± 0.6 (0.293)
GNP@PDA-2	50.6 ± 5.9	108.4 ± 6.5	26.7 ± 2.5	175.4 ± 3.0 (0.179)
GNP@PDA-3		131.3 ± 8.5	36.4 ± 3.6	335.3 ± 5.1 (0.211)

[a] The values were calculated from TEM images by Image J software. [b] The values were obtained from DLS measurements of particles in Milli-Q water and given in mean ± SD (PDI: polydispersity index) of triple measurements.

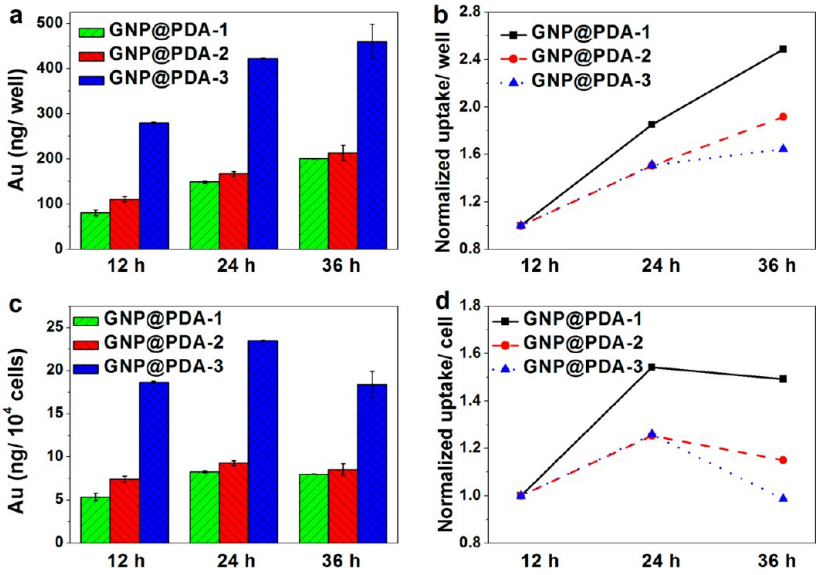

Figure 2. (a) Cellular uptake of GNP@PDA per well by HepG2 cells at time points of 12, 24, and 36 h. (b) Normalized uptake of GNP@PDA per well at different points of time to that at 12 h. (c) Cellular uptake of GNP@PDA per cell by HepG2 cells at time points of 12, 24, and 36 h. (d) Normalized uptake of GNP@PDA per cell at different points of time to that at 12 h. Error bars represent mean ± SD (n = 3).

solution. It suggested that the GNP@PDA with thicker shell resulted in a large size with weak colloidal stability. The smaller GNP@PDA-1 also showed better stability than the larger GNP@PDA-3 in biological media such as serum-supplemented cell culture media (Table S2 and Figure S3, Supporting Information). Moreover, all of the GNP@PDA in serum-supplemented cell culture media showed better stability than that in serum-free media. The GNP@PDA were not stable in the cell culture media with high ionic strength, but their stability was improved in the serum-supplemented media because of the protein adsorption on the NPs.[62,63]

Interactions between GNP@PDA and Cells *in Vitro*. To study the interactions between cells and nanoparticles with PDA surface, we first examined the cytotoxicity of these GNP@PDA particles with different shell thicknesses by using MTT assay. The results showed all three kinds of GNP@PDA with different sizes had no detectable cytotoxicity on HepG2 cells with a concentration of gold up to 20 mg/L (Figure S4, Supporting Information). Our observation agreed well with many reports in which PDA exhibited no cytotoxicity.[38,45,47] Next, we investigated the cellular uptake of these GNP@PDA particles by cancer cell HepG2. The uptake of GNP@PDA was quantified at time points of 12, 24, and 36 h by determining the gold quantity within cells by ICP-MS (Figure 2). We found that the uptake per well increased when prolonged the incubation time from 12 to 36 h for all three kinds of GNP@PDA (Figure 2a). It indicates that the PDA coatings can smoothly translocate nanoparticles into cancer cells. The uptake of large particles was higher than that of small particles; in particular, the uptake of GNP@PDA-3 was much higher than that of GNP@PDA-1 or GNP@PDA-2. It was observed that the uptake by cells is the highest for GNP@PDA-3 and the lowest for GNP@PDA-1 at all three points of time. However, when the uptake of particles at different points of time was normalized to that at the point of 12 h, we found that the increased ratio of cell uptake was the highest for GNP@PDA-1 and was the lowest for GNP@PDA-3 (Figure 2b). GNP@PDA-3 had a high uptake at time of 12 h incubation and then increased ~40% at time of 24 h incubation, which was almost saturated and increased very slowly when time was prolonged to 36 h. The uptake of GNP@PDA-2 and GNP@PDA-1 increased linearly with time. Here, the three kinds of GNP@PDA had the same surface composition and had similar zeta potential when incubated in cell culture media containing fetal bovine serum (10% FBS, ~ −20 mV, Table S1, Supporting Information). Although nanoparticle size might affect their endocytosis, in this work, the sedimentation of GNP@PDA played a main role in causing the uptake differences among these particles. The GNP@PDA with a thicker shell showed weaker stability in the cell culture media, which resulted in large aggregates and were more likely to sedimentate on the cells (Figure S3 and Table S2, Supporting Information). The sedimentation of particles would result in high local concentration of NPs on the cell surfaces and enhance the direct interaction between NPs and cells,[61,64] which led to fast and high uptake of GNP@PDA-3 compared to GNP@PDA-2 or GNP@PDA-1. When dividing the uptake to cell number, the uptake per cell of GNP@PDA all increased at time from 12 to 24 h, and decreased from 24 to 36 h (Figure 2c,d). This phenomenon resulted from the cell division during incubation where

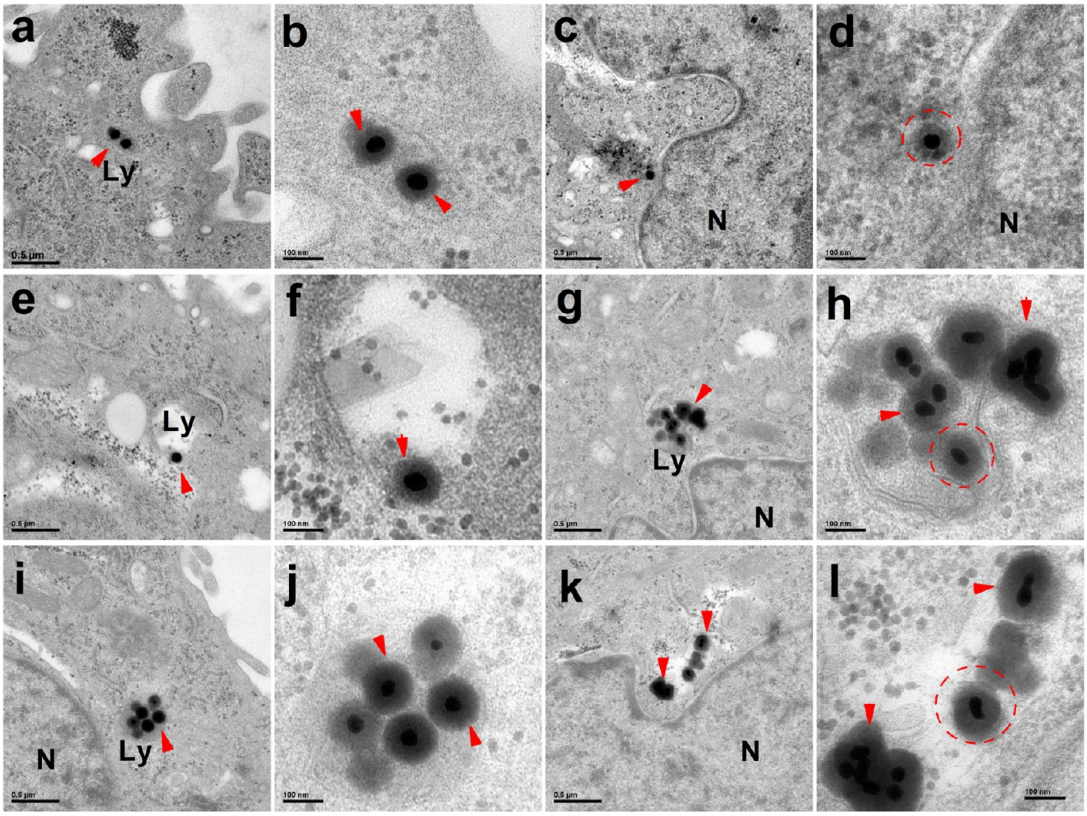

Figure 3. Representative TEM section images of HepG2 cells after incubation with GNP@PDA-1 (a−d), GNP@PDA-2 (e−h), and GNP@PDA-3 (i−l) for 24 h. The images in the second column are high magnification of images in the first column; the images in the fourth column are high magnification of images in the third column. Red arrows and circles mark the particles. N: nucleus, C: cytosol, Ly: lysosome.

the cell proliferation rate exceeded the nanoparticle endocytosis rate.

To further elucidate the intracellular existence status of GNP@PDA within cells, ultrathin cell section TEM analysis was carried out.[65] As shown in Figure 3, more GNP@PDA-3 particles were found internalized into cells than GNP@PDA-1 or GNP@PDA-2; these results were consistent with the uptake quantified by ICP-MS. The small GNP@PDA-1 were more likely to localize in cells as individual particles, while large GNP@PDA-3 were more likely to exist as clusters of several particles together (Figure 3, Figures S5−S7, Supporting Information). As quantitative chemical analysis cannot distinguish the different locations of particles inside the cell,[66] the numbers of particles presented together in a lysosome or cytosol at the same position were obtained by counting the particles present in one representative section (Figure S8, Supporting Information). It showed that ∼65% of sites with GNP@PDA-1 were one particle in one lysosome or cytosol, while ∼70% of sites with GNP@PDA-3 were clusters of more than two particles together. It can be explained by the stability of GNP@PDA in cell culture media, where most of GNP@PDA-1 were stable as monodisperse particles, while GNP@PDA-3 were less stable and tended to form small aggregates (Table S2, Supporting Information).

It was observed that many of GNP@PDA localized in the lysosomes within cells (Figure 3, Figures S5−S7, Supporting Information), which suggested that the cell internalization of GNP@PDA followed the endocytosis uptake mechanism.[9] Interestingly, some of nanoparticles distributed in the cytosol without vesicle structures wrapped rather than were trapped in the lysosomes (Figure 3c, Figures S6c and S7d, Supporting Information). It indicated that the GNPs with a PDA shell can partly escape from the endosomes/lysosomes. There are many amino groups on the PDA shell, which might lead to the endosomal escape of nanoparticles by proton sponge effect.[67] In addition, many of nanoparticles were found close to the nucleus, though no NPs were observed in nucleus (Figure 3c,j,k). Despite that the mechanism for perinuclear localization of these PDA-coated NPs is not clear yet, this property can give rise to a higher concentration of delivery agents around the nucleus. These findings suggested that polydopamine coating could make the modified nanostructures partially escape from the endosomes/lysosomes to cytosol and appear closely to the nucleus, which may bring a greater efficacy of the cytoplasmic as well as nuclear delivery of nanocarriers.

Additionally, we found that the core/shell structures of GNP@PDA did not change notably in the lysosomes or cytosol within cells during an incubation period of

24 h (Figure 3). The PDA shells were clearly proven by the TEM images, and their thicknesses were the same as that before cell incubation. It indicated that the PDA shell was quite stable under this *in vitro* condition. It was reported that the PDA was degradable in the presence of hydrogen peroxide,[59,60] an endogenous molecule produced by reduced nicotinamide adenine dinucleotide phosphate (NADPH) oxidases, which widely exist in phagocytes and many organs.[59] We also found that the PDA shell was not stable in presence of hydrogen peroxide; the shell degraded completely in one week (Figure S9, Supporting Information). The remaining question is whether the PDA is stable *in vivo*.

Fate of GNP@PDA *in Vivo*. To carry out *in vivo* studies, we prepared GNP@PDA with a uniform thin shell of 10.3 ± 1.1 nm (Figure 4a,b), which had good stability for high concentration (>1 mg Au/mL) and long time storage (at least 4 months). First, we investigated the kinetics of GNP@PDA circulation in the bloodstream after being intravenously injected into mice. The blood circulation curve of the GNP@PDA is shown in Figure 4c (given in % ID). It revealed that only ~15% of injected NPs remained in the blood at 5 min postinjection (p.i.), which indicated most of GNP@PDA were quickly cleared out from blood. As time increased the NPs in blood gradually decreased, which can be fitted to a monoexponential decay model, resulting in a half-decay time ($t_{1/2}$) of ~4.9 ± 1.1 h. For the biodistribution of GNP@PDA in main organs, it was found that NPs accumulated in the liver and spleen with much higher quantity than in the heart, kidneys, and lung as expected because of the strong phagocytosis in reticuloendothelial system (RES) organs (Figure 4d). The highest accumulation of NPs were found in the liver (~40% ID), followed by the spleen (~13% ID). Considering that the spleen is much smaller than the liver, the concentration of GNP@PDA in the spleen was much higher than that in the liver (~100 *vs* ~30% ID/g). For these PDA-coated GNPs, once they enter the bloodstream, they are susceptible to nonspecific plasma protein adsorption, known as opsonization.[68] The opsonized nanoparticles can be easily captured by the RES or mononuclear phagocytic system (MPS), leading to a rapid clearance of nanoparticles from blood. Therefore the quantity of GNP@PDA in blood drastically reduced within only 5 min p.i. The liver and spleen, which contain a lot of phagocytes, are two main organs in the RES; it is reasonable that they had such high accumulation of GNP@PDA. After six weeks p.i., the biodistribution of GNP@PDA in main organs did not change much (Figure 4d), which demonstrated that these PDA-coated GNPs captured by the RES organs were difficult to clear out, even over a long period. For an *in vivo* application such as drug delivery to tumors, prolonging blood circulation, reducing nonspecific accumulation, and enhancing targeting efficiency of nanoparticles are desirable. It is well-known that the

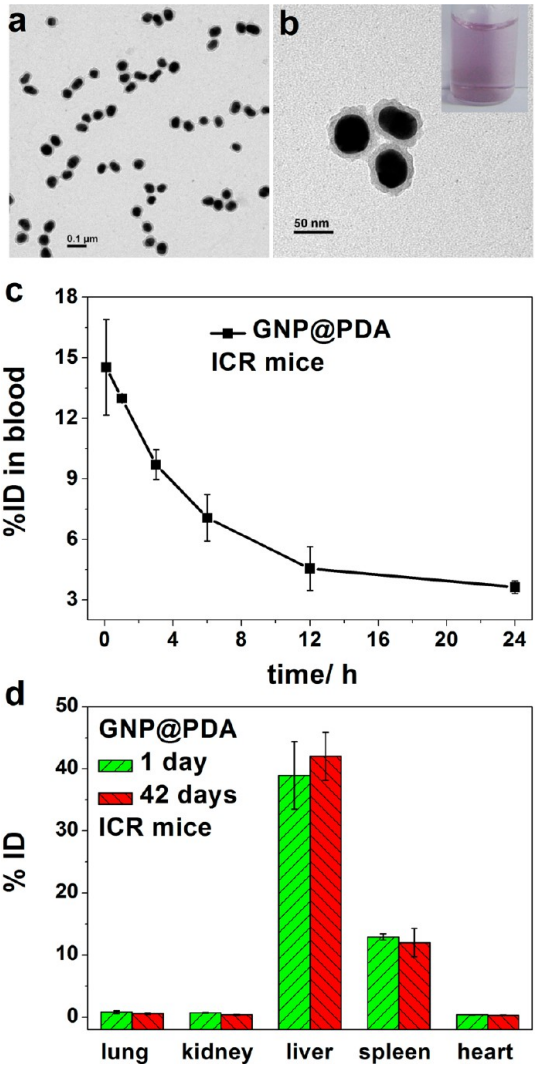

Figure 4. (a,b) Representative TEM images of GNP@PDA used for *in vivo* study (inset: digital image of diluted solution of GNP@PDA with an Au concentration of 20 mg/L). (c) The blood circulation curve of GNP@PDA. (d) Biodistribution of GNP@PDA in main organs at one day and six weeks post-injection (p.i.).

PDA coating has latent reactivity toward amine and thiol groups, which endows it with great possibility for secondary modification. It is believed that the secondary modification of PDA will improve their properties in many applications *in vivo* as applied for *in vitro* studies.[45,46,50] In present work, we mainly focused on the direct interactions between PDA surface and biosystems, so GNPs with PDA shell with further modification are yet to be studied.

As shown above, there are very high uptake of GNP@PDA in the liver and spleen. We further investigated the uptake of NPs in the two organs by TEM analysis. In the liver, it was observed that GNP@PDA mainly accumulated in Kupffer cells, while no NPs were found in hepatocytes whether at 1 day or 42 days p.i. (Figures S10, S11, Supporting Information). Unlike the liver, the spleen hosts a number of cell types in addition

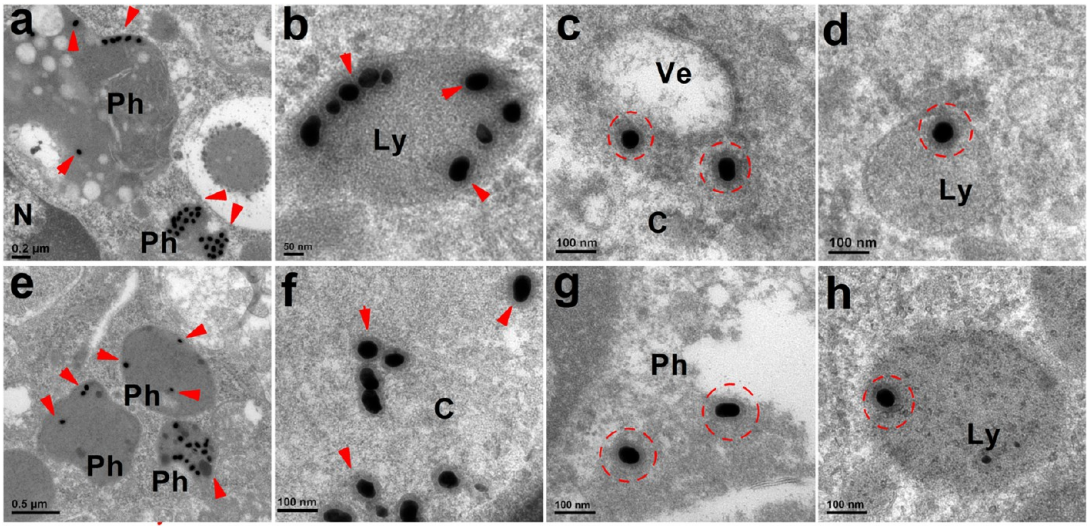

Figure 5. Representative TEM section images of the liver after injection of GNP@PDA for 1 day (a−d) and 42 days (e−h). Red arrows and circles mark the particles. N: nucleus, C: cytosol, Ly: lysosome, Ph: phagolysosome, Ve: vesicle.

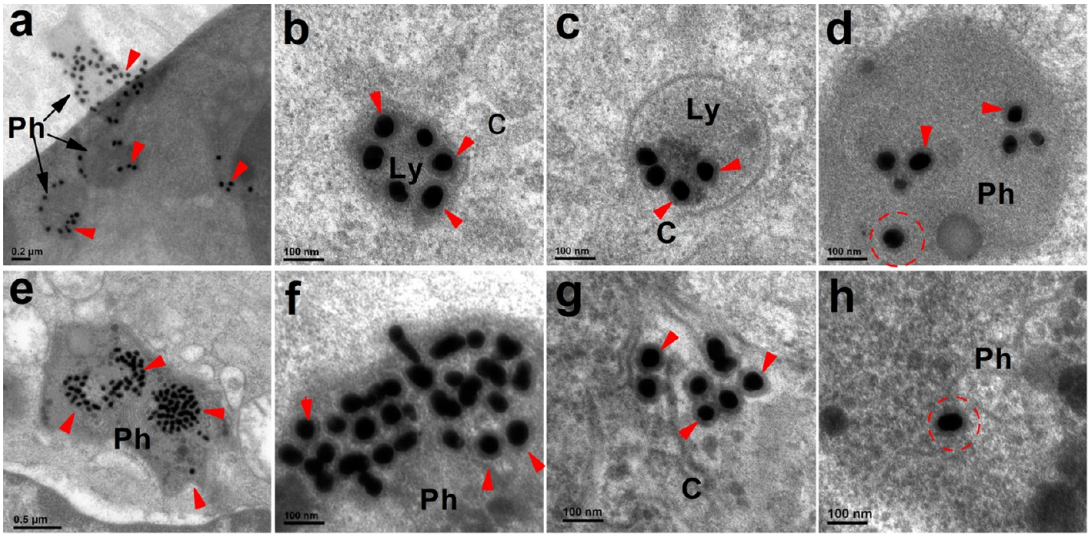

Figure 6. Representative TEM section images of the spleen after injection of GNP@PDA for 1 day (a−d) and 42 days (e−h). Red arrows and circles mark the particles. C: cytosol, Ly: lysosome, Ph: phagolysosome.

to the macrophages including reticular cells, lymphocytes, and a variety of dendritic cells.[69] From the TEM images, we found that the GNP@PDA mainly accumulated in macrophages with rare uptake in lymphocytes (Figures S12, S13, Supporting Information). In addition, GNP@PDA uptake in granulocytes (Figure S14, Supporting Information), reticular cells (Figure S15, Supporting Information), and plasma cells (Figure S16, Supporting Information) was observed. Some NPs accumulating near the capillary vessel in the spleen were also found (Figure S17, Supporting Information). Moreover, there were GNP@PDA accumulating in erythrocytes that were phagocytosed by macrophages (Figure S18, Supporting Information). It indicates that when the NPs were injected into blood, some of the NPs were uptaken by erythrocytes, which then were captured in the spleen. Intracellular localization of GNP@PDA *in vivo* can be clearly observed from the ultrathin TEM section images because of the high contrast of gold core. In the liver, the GNP@PDA accumulating in Kupffer cells mainly located in phagolysosomes because of the strong phagocytosis process (Figure 5a,e,g). Many NPs were also located in lysosomes (Figure 5b,d,h), which indicated the pinocytosis of GNP@PDA by the Kupffer cells also existed. Furthermore, the GNP@PDA in cytosol (Figure 5c,f) were found, which confirmed the ability of these PDA-coated NPs to escape from lysosomes and accomplish cytosol delivery. Similar intracellular status of GNP@PDA was found in the spleen. The NPs accumulated in cells of the spleen were mainly located in phagolysosomes (Figure 6a,d−f,h), and they were also found in lysosomes (Figure 6b,c) and cytosol (Figure 6g). No NPs were found in mitochondria or

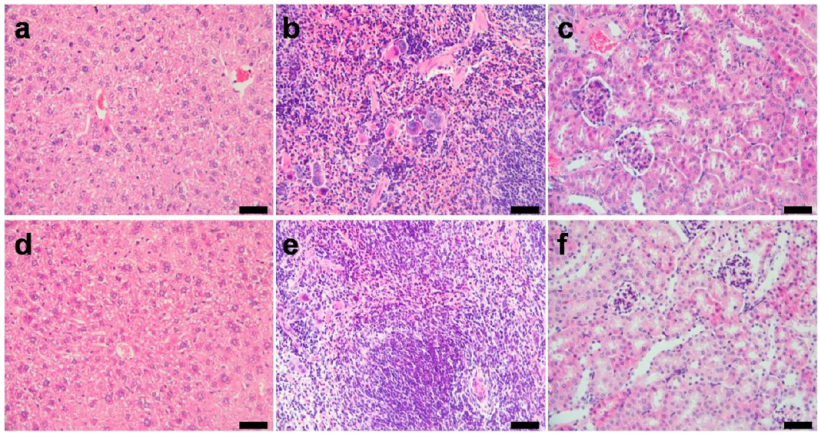

Figure 7. Representative H&E stained images of major organs including liver (a,d), spleen (b,e), and kidneys (c,f) of male ICR mice after a single injection of GNP@PDA for 1 day (a−c) and 42 days (d−f). No notable organ damage or lesions were observed for GNP@PDA treated mice. Scale bar is 20 μm.

nucleus of cells in the liver or spleen. This detailed information for cellular and intracellular distribution of PDA-coated NPs in immune cells would be helpful to design nanoparticle-medicated immunotherapy.[70,71]

While doing *in vitro* study, we found the PDA shell retained in HepG2 cells after 24 h incubation (Figure 3). Here, the *in vivo* results showed that the thickness of PDA shell on GNPs also did not change notably in the liver or spleen from one day to six weeks after injection (Figure 5, Figure 6). It strongly suggested that the PDA shells are quite stable *in vivo* and undegradable at least in a short period. Sometimes, a material used *in vivo* is desired to be degradable in the body in order to be eventually cleared out. However, PDA as a coating for surface modification and its stability *in vivo* for a certain period could be advantages in many applications. For an example, the application of PDA as molecularly imprinted polymer should be greatly beneficial from the excellent stability of the PDA shell, which could keep the imprinted sites with precise physical shapes under various complex biological conditions for a long time.[34,39,41] In another case, the excellent stability of PDA coating will enable it to afford durable surface properties to the modified devices when used *in vivo*, such as the scaffold for tissue engineering.[31,32,36,54,55] Furthermore, dopamine has been reported to be highly cytotoxic,[72,73] while the polydopamine showed good biocompatibility both *in vitro*[38,45,47,54−57,74] and *in vivo*.[36,59] Hong *et al.* reported that PDA coating greatly reduced the immunological responses of blood on quantum dots.[36] It was postulated that the toxic Cd ions leaching from the core of QDs could be captured by the PDA nanolayer, improving blood compatibility. Liu *et al.* showed that PDA nanoparticles had good tissue and blood compatibility over a long time.[59] Here we also found the GNP@PDA had no notable histological toxicity on the main organs up to six weeks after a single intravenous injection (Figure 7). Therefore, the PDA surface modification could be a universal strategy to reduce the toxicity of materials. Especially for many nanomaterials containing high toxic component, a compact PDA nanolayer with high stability *in vivo* would effectively reduce the potential detrimental effect of those nanoparticles on the body, which is induced by the possible leaching of the toxic element.[14]

CONCLUSION

In summary, we demonstrated that the mussel-inspired PDA nanoshells on GNPs were very stable *in vivo*. We simply modified GNPs with well controlled PDA nanolayers to form uniform core/shell nanostructures. The PDA-coated GNPs showed low cytotoxicity and could smoothly translocate to cancer cells. TEM analysis demonstrated that the PDA nanoshells were intact within cells after 24 h of incubation. Intracellular localization of GNP@PDA showed that PDA coating can make the modified nanostructures partially escape from the endosomes/lysosomes to cytosol and locate close to the nucleus. It suggests that the PDA modification is very promising for future novel nanocarriers delivery methods. *In vivo* study showed that the GNP@PDA in the liver were mainly uptaken by the Kupffer cells but uptaken by a variety of cells in the spleen. The detailed information of uptake in immune cells would be helpful to design nanoparticle-medicated cancer immunotherapy. Importantly, the PDA nanoshells were demonstrated to be stable within cells of the liver and spleen for up to six weeks, which strongly supports the excellent stability of PDA *in vivo*. Moreover, the GNP@PDA showed no notable histological toxicity for a long time. These results strongly suggest that the PDA surface modification can serve as an effective strategy to form an ultrastable nanolayer on materials and improve their biocompatibility for *in vivo* application. Meanwhile, the stable PDA

nanolayers can further react with thiol- and amino-terminated molecules, which will facilitate the design of multifunctional nanomedical platforms for bioapplication.

EXPERIMENTAL SECTION

Materials. Dopamine hydrochloride and 3-(4,5-dimethylthiazol-2-yl)-2,5-diphenyltetrazolium bromide (MTT) were purchased from Sigma-Aldrich. Hydrogen tetrachloroaurate hydrate ($HAuCl_4 \cdot 4H_2O$), trisodium citrate dihydrate ($C_6H_5Na_3O_7 \cdot 2H_2O$), and other regents were purchased from Sinopharm Chemical Reagent Co., Ltd. Cell line HepG2 was purchased from China Center for Typical Culture Collection, and all reagents for the cell culture were used directly after being purchased. All water was distilled and subsequently purified to Millipore Milli-Q quality. For nanoparticle synthesis, all glassware used was cleaned by freshly prepared aqua regia solution (HCl/HNO_3, 3:1). For cell experiments, all of the solutions and substrates were sterilized in advance.

Synthesis of Citrate Protected Gold Nanoparticles (GNPs). Citrate-capped GNPs (GNP-Cit) in diameter of ~50 nm were synthesized according to the reference with minor modifications.[75] Briefly, 1.214 mL of 10 mM $HAuCl_4$ was added to 50 mL of Milli-Q water, and the solution was heated to boiling. Next, 0.5 mL of 10 mg/mL citrate sodium solution was added to the solution, which was refluxed for half an hour as the color changed from dark blue to red. After being cooled to room temperature, these GNPs were modified with dopamine.

Synthesis of Polydopamine (PDA) Coated GNPs. For *in vitro* study, we prepared three kind of PDA-coated GNPs (GNP@PDA) with different shell thickness by adjusting the concentration of dopamine in the reaction. In the following discussion, we refer the particles obtained from the dopamine solution with final concentrations of 0.1, 0.2, and 0.4 mg/mL as GNP@PDA-1, GNP@PDA-2, and GNP@PDA-3, respectively. Briefly, 17 mL of above GNP-Cit solution was added to 17 mL of freshly prepared dopamine solution in Tris buffer (10 mM, pH 8.5). After being stirred under air at room temperature for 1 h, the modified GNPs were purified by centrifugation and redispersed in water. Then the GNP@PDA were further filtrated through syringe filters with cellulose acetate membranes with a pore size of 1 μm to remove the bigger impurities like PDA accumulates and GNP@PDA aggregates.

Characterization of GNP@PDA. UV−vis analysis was carried out with a UV−vis Shimadzu UV-2505 spectrometer using 1-cm-path length quartz cuvettes. Spectra were collected within the range of 400−800 nm. When detecting the spectra of GNPs in cell culture medium, Dulbecco's Modified Eagle Medium (DMEM) supplemented with 10% fetal bovine serum (FBS) without phenol red was used to exclude the strong absorbance of phenol red. Transmission electron microscopy (TEM) analysis was performed on a JEM-1230EX TEM operating at 80 kV in bright field mode. For the determination of particle size, over 100 particles were counted in multiple pictures from different areas of the TEM grid. Dynamic light scattering (DLS) analysis was performed on 90plus/BI-MAS (90 Plus Particle Size Analyzer, Brookhaven Instruments Co.). The scattering angle was kept at 90°, and the wavelength in the vacuum was set as 633 nm during the whole experiment. Zeta potential measurements were also performed on a Delsa Nano C particle analyzer (Beckman Coulter Ireland, Inc.).

Cell Culture. HepG2 cells were cultured with regular growth medium consisting of high-glucose DMEM supplemented with 10% fetal bovine serum (FBS), 100 U/mL of penicillin, and 100 mg/mL of streptomycin and cultured at 37 °C in a 5% CO_2 humidified environment.

Cytotoxicity. Cytotoxicity was performed by standard MTT assay. The colorimetric MTT test assesses cell metabolic activity based on the ability of the mitochondrial succinate/tetrazolium reductase system to convert the yellow dye (MTT) to a purple formazan in living cells. The metabolic activity of the cell is proportional to the color density formed. To determine the relative cell viability by MTT assay, cells were plated at a density of 5×10^3 cells per well in a 96-well plate and cultured for 24 h. The medium was replaced with fresh medium containing the GNP@PDA of varying concentrations (given in Au atomic concentration, which was determined by inductively coupled plasma mass spectrometry (ICP-MS, Thermo Elemental Corporation of USA, XSeries II)). Cells cultured in nanoparticle-free media were used as a control. After treatment for 24 h, the wells were washed with phosphate buffered saline (PBS, ~0.15 M NaCl, pH 7.4; to rule out the interference from MTT interacts with GNPs in the suspension), the medium was replaced with 100 μL of fresh medium, 20 μL of MTT (5 mg/mL) was added to each well, and the cells were further cultured at 37 °C for 4 h. The dark blue formazan crystals generated by the mitochondria dehydrogenase in live cells were dissolved with 150 μL of dimethyl sulfoxide to measure the absorbance at 570 nm by a microplate reader (model 550, Bio Rad). The relative cell viability (%) = the absorption of treated well/the absorption of control well × 100%.

Internalization of GNP@PDA Detected by ICP-MS Analysis. Cellular uptake of the GNP@PDA was determined by ICP-MS quantitatively. HepG2 cells were seeded on a 24-well plate at a density of 1×10^5 cells per well and cultured for 24 h. Then, cells were incubated with GNP@PDA (added 20 μL of GNP@PDA solution into 480 μL of fresh culture medium; final concentration of Au was 5 mg/L) for 12, 24, and 36 h. In all the processes, the cells are cultured in the medium with 10% FBS. At determined time, the cells were washed five times with PBS and then treated by aqua regia ($HCl:HNO_3$ =1:3, volume ratio) for 2 h. The treated solution was diluted to determine Au concentration by ICP-MS. The Au amount per well data from ICP-MS analysis are presented as mean ± standard deviation (SD) for experiments repeated three times. Divided by the number of cells, the data of Au amount per cell was calculated.

Intracellular Fate of GNP@PDA Detected by TEM Analysis. For TEM cell sections analysis, the cells were seeded on a 6-well plate at a density of 5×10^5 cells per well. After being cultured for 24 h, the medium was replaced with fresh medium, and then the cells were incubated with GNP@PDA with a Au atomic concentration of 5 mg/L for 24 h. At the determined time, the cells were washed five times with PBS and trypsizined, centrifuged, and then fixed with 2.5% glutaradyhyde. After 2 h of fixation at 4 °C, the samples were washed with phosphate buffer (0.1 M, pH 7.0) three times. Then the samples were fixed with 1% perosmic oxide for 2 h at 4 °C. After being washed in water, the samples were dehydrated in an alcohol series, embedded, and sliced with the thickness between 50 and 70 nm.

Synthesis of GNP@PDA for *in Vivo* Study. Briefly, 300 mL of GNP-Cit solution was added to 300 mL of 0.2 mg/mL freshly prepared dopamine solution in Tris buffer (10 mM, pH 8.5). After being stirred under air at room temperature for 1 h, the modified GNPs were purified twice by centrifugation and redispersed in water. The GNP@PDA were filtrated through syringe filters with cellulose acetate membranes with a pore size of 1 μm. The Au concentration of GNP@PDA was measured by ICP-MS.

Animals. Animal experiments were performed according to Guidelines for Animal Care and Use Committee, Zhejiang University. Healthy male ICR mice were purchased from animal center of Zhejiang Academy of Medical Sciences.

Blood Circulation and Biodistribution of GNP@PDA. GNP@PDA given in 0.1 mL of solution with 100 μg Au was injected *via* the tail vein in each mouse (male ICR mice, 18−22 g). Blood circulation analysis was performed by measuring the remaining gold content from blood taken after injection at different time. Blood samples were collected at 5 min, 1, 3, 6, 12, and 24 h postinjection (p.i.); the total blood weight was estimated to be ~7% of body weight. Biodistribution analysis was performed by measuring the gold content in main organs including the liver, kidneys, spleen, heart, and lung, collected at 1 day and 42 days

p.i. The gold content was analyzed by ICP-MS. The intracellular localization of GNP@PDA in the liver and spleen was investigated by TEM analysis.

ICP-MS Measurement. Organs were washed in PBS, weighted, and lyophilized for 1 day. Blood was lyophilized directly. The dried tissues and blood were mashed and dissolved in aqua regia for 24 h. Then the aqua regia was diluted, and the precipitated tissue debris was removed by centrifugation at 10 000 rpm for 5 min. The Au content in the supernatant was detected by ICP-MS.

TEM Analysis. Organs were first fixed in 2.5% glutaraldehyde (in 0.1 M phosphate buffer, pH 7.0). Then the samples were fixed with 1% perosmic oxide for 2 h at 4 °C. After being washed in water, the samples were dehydrated in an alcohol series, embedded, and sliced with the thickness between 50 and 70 nm. TEM analysis was performed on a JEM-1230EX TEM operating at 80 kV in bright field mode.

Histological Examinations. For histology, mice were sacrificed at 1 day and 42 days p.i., and major organs (liver, kidneys and spleen) were harvested. Organs were fixed in 3.7% neutral buffered formalin, processed routinely into paraffin, sectioned into 4 μm, and stained with hematoxylin and eosin (H&E). The histology was performed in a blinded fashion by professional personnel in the medical college of Zhejiang University. The samples were examined by microscope (Olympus BX61 Inverted Microscope) in bright-field.

Conflict of Interest: The authors declare no competing financial interest.

Acknowledgment. Financial support from the National Science Fund for Distinguished Young Scholars (51025312), the National Basic Research Program of China (2011CB606203), NSFC-50830106, 51333005, 21174126, and Open Project of State Key Laboratory of Supramolecular Structure and Materials (SKLSSM 201204, SKLSSM 201316), and Research Fund for the Doctoral Program of Higher Education of China (20110101110037, 20110101120049, and 20120101130013) is gratefully acknowledged. We would like to thank G. Tang and J. Zhou for animal experiments, Y. Xu and H. Wang for TEM, and Z. Xu for ICP-MS.

Supporting Information Available: Supporting experimental results, Tables S1 and S2, and Figures S1−S18. This material is available free of charge *via* the Internet at http://pubs.acs.org.

REFERENCES AND NOTES

1. Daniel, M. C.; Astruc, D. Gold Nanoparticles: Assembly, Supramolecular Chemistry, Quantum-Size-Related Properties, and Applications toward Biology, Catalysis, and Nanotechnology. *Chem. Rev.* **2004**, *104*, 293–346.
2. Sperling, R. A.; Rivera Gil, P.; Zhang, F.; Zanella, M.; Parak, W. J. Biological Applications of Gold Nanoparticles. *Chem. Soc. Rev.* **2008**, *37*, 1896–1908.
3. Giljohann, D. A.; Seferos, D. S.; Daniel, W. L.; Massich, M. D.; Patel, P. C.; Mirkin, C. A. Gold Nanoparticles for Biology and Medicine. *Angew. Chem., Int. Ed.* **2010**, *49*, 3280–3294.
4. Barreto, J. A.; O'Malley, W.; Kubeil, M.; Graham, B.; Stephan, H.; Spiccia, L. Nanomaterials: Applications in Cancer Imaging and Therapy. *Adv. Mater.* **2011**, *23*, H18–H40.
5. Pelaz, B.; Jaber, S.; Jimenez de Aberasturi, D.; Wulf, V.; Aida, T.; De la Fuente, J. M.; Feldmann, J.; Gaub, H. E.; Josephson, L.; Kagan, C. R.; *et al.* The State of Nanoparticle-Based Nanoscience and Biotechnology: Progress, Promises, and Challenges. *ACS Nano* **2012**, *6*, 8468–8483.
6. Dreaden, E. C.; Alkilany, A. M.; Huang, X.; Murphy, C. J.; El-Sayed, M. A. The Golden Age: Gold Nanoparticles for Biomedicine. *Chem. Soc. Rev.* **2012**, *41*, 2740–2779.
7. Saha, K.; Agasti, S. S.; Kim, C.; Li, X.; Rotello, V. M. Gold Nanoparticles in Chemical and Biological Sensing. *Chem. Rev.* **2012**, *112*, 2739–2779.
8. Qiao, R.; Zeng, J.; Jia, Q.; Du, J.; Shen, L.; Gao, M. Magnetic Iron Oxide Nanoparticle-an Important Footstone towards MR Molecular Imaging of Tumor. *Acta Phys.-Chim. Sin.* **2012**, *28*, 993–1011.
9. Verma, A.; Stellacci, F. Effect of Surface Properties on Nanoparticle-Cell Interactions. *Small* **2010**, *6*, 12–21.
10. Gong, Y. K.; Winnik, F. M. Strategies in Biomimetic Surface Engineering of Nanoparticles for Biomedical Applications. *Nanoscale* **2012**, *4*, 360–368.
11. Quarta, A.; Curcio, A.; Kakwere, H.; Pellegrino, T. Polymer Coated Inorganic Nanoparticles: Tailoring the Nanocrystal Surface for Designing Nanoprobes with Biological Implications. *Nanoscale* **2012**, *4*, 3319–3334.
12. Zhang, F.; Lees, E.; Amin, F.; Rivera_Gil, P.; Yang, F.; Mulvaney, P.Parak, W. J. Polymer-Coated Nanoparticles: A Universal Tool for Biolabelling Experiments. *Small* **2011**, *7*, 3113–3127.
13. Zhao, F.; Zhao, Y.; Liu, Y.; Chang, X.; Chen, C.; Zhao, Y. Cellular Uptake, Intracellular Trafficking, and Cytotoxicity of Nanomaterials. *Small* **2011**, *7*, 1322–1337.
14. Zhu, M.; Nie, G.; Meng, H.; Xia, T.; Nel, A.; Zhao, Y. Physicochemical Properties Determine Nanomaterial Cellular Uptake, Transport, and Fate. *Acc. Chem. Res.* **2013**, *46*, 622–631.
15. Qiao, R.; Jia, Q.; Hüwel, S.; Xia, R.; Liu, T.; Gao, F.; Galla, H. J.; Gao, M. Receptor-Mediated Delivery of Magnetic Nanoparticles across the Blood-Brain Barrier. *ACS Nano* **2012**, *6*, 3304–3310.
16. Na, H. B.; Palui, G.; Rosenberg, J. T.; Ji, X.; Grant, S. C.; Mattoussi, H. Multidentate Catechol-Based Polyethylene Glycol Oligomers Provide Enhanced Stability and Biocompatibility to Iron Oxide Nanoparticles. *ACS Nano* **2012**, *6*, 389–399.
17. Liu, X.; Huang, H.; Liu, G.; Zhou, W.; Chen, Y.; Jin, Q.; Ji, J. Multidentate Zwitterionic Chitosan Oligosaccharide Modified Gold Nanoparticles: Stability, Biocompatibility and Cell Interactions. *Nanoscale* **2013**, *5*, 3982–3991.
18. Pastoriza-Santos, I.; Pérez-Juste, J.; Liz-Marzán, L. M. Silica-Coating and Hydrophobation of CTAB-Stabilized Gold Nanorods. *Chem. Mater.* **2006**, *18*, 2465–2467.
19. Kim, J.; Kim, H. S.; Lee, N.; Kim, T.; Kim, H.; Yu, T.; Song, I. C.; Moon, W. K.; Hyeon, T. Multifunctional Uniform Nanoparticles Composed of a Magnetite Nanocrystal Core and a Mesoporous Silica Shell for Magnetic Resonance and Fluorescence Imaging and for Drug Delivery. *Angew. Chem., Int. Ed.* **2008**, *120*, 8566–8569.
20. Ghosh Chaudhuri, R.; Paria, S. Core/Shell Nanoparticles: Classes, Properties, Synthesis Mechanisms, Characterization, and Applications. *Chem. Rev.* **2011**, *112*, 2373–2433.
21. Lee, H.; Dellatore, S. M.; Miller, W. M.; Messersmith, P. B. Mussel-Inspired Surface Chemistry for Multifunctional Coatings. *Science* **2007**, *318*, 426–430.
22. Lee, H.; Rho, J.; Messersmith, P. B. Facile Conjugation of Biomolecules onto Surfaces *via* Mussel Adhesive Protein Inspired Coatings. *Adv. Mater.* **2009**, *21*, 431–434.
23. Kang, S. M.; You, I.; Cho, W. K.; Shon, H. K.; Lee, T. G.; Choi, I. S.; Karp, J. M.; Lee, H. One-Step Modification of Superhydrophobic Surfaces by a Mussel-Inspired Polymer Coating. *Angew. Chem., Int. Ed.* **2010**, *49*, 9401–9404.
24. Lynge, M. E.; van der Westen, R.; Postma, A.; Städler, B. Polydopaminea Nature-Inspired Polymer Poating for Biomedical Science. *Nanoscale* **2011**, *3*, 4916–4928.
25. Ye, Q.; Zhou, F.; Liu, W. Bioinspired Catecholic Chemistry for Surface Modification. *Chem. Soc. Rev.* **2011**, *40*, 4244–4258.
26. Xi, Z.-Y.; Xu, Y.-Y.; Zhu, L.-P.; Wang, Y.; Zhu, B.-K. A Facile Method of Surface Modification for Hydrophobic Polymer Membranes Based on the Adhesive Behavior of Poly (DOPA) and Poly (Dopamine). *J. Membr. Sci.* **2009**, *327*, 244–253.
27. Jiang, J.; Zhu, L.; Zhu, L.; Zhu, B.; Xu, Y. Surface Characteristics of a Self-Polymerized Dopamine Coating Deposited on Hydrophobic Polymer Films. *Langmuir* **2011**, *27*, 14180–14187.
28. Yang, S. H.; Kang, S. M.; Lee, K.-B.; Chung, T. D.; Lee, H.; Choi, I. S. Mussel-Inspired Encapsulation and Functionalization of Individual Yeast Cells. *J. Am. Chem. Soc.* **2011**, *133*, 2795–2797.
29. Mangindaan, D.; Yared, I.; Kurniawan, H.; Sheu, J. R.; Wang, M. J. Modulation of Biocompatibility on Poly(Vinylidene Fluoride) and Polysulfone by Oxygen Plasma Treatment and Dopamine Coating. *J. Biomed. Mater. Res., Part A* **2012**, *100*, 3177–3188.

30. Faure, E.; Falentin-Daudré, C.; Jérôme, C.; Lykawa, J.; Fournier, D.; Woisel, P.; Detrembleur, C. Catechols as Versatile Platforms in Polymer Chemistry. *Prog. Polym. Sci.* **2013**, *38*, 236–270.
31. Faure, E.; Falentin-Daudré, C.; Lanero, T. S.; Vreuls, C.; Zocchi, G.; Van De Weerdt, C.; Martial, J.; Jérôme, C.; Duwez, A. S.; Detrembleur, C. Functional Nanogels as Platforms for Imparting Antibacterial, Antibiofilm, and Antiadhesion Activities to Stainless Steel. *Adv. Funct. Mater.* **2012**, *22*, 5271–5282.
32. Faure, E.; Vreuls, C.; Falentin-Daudré, C.; Zocchi, G.; Van de Weerdt, C.; Martial, J.; Jérôme, C.; Duwez, A.-S.; Detrembleur, C. A Green and Bio-Inspired Process to Afford Durable Anti-Biofilm Properties to Stainless Steel. *Biofouling* **2012**, *28*, 719–728.
33. Fei, B.; Qian, B.; Yang, Z.; Wang, R.; Liu, W.; Mak, C.; Xin, J. H. Coating Carbon Nanotubes by Spontaneous Oxidative Polymerization of Dopamine. *Carbon* **2008**, *46*, 1795–1797.
34. Zhou, W. H.; Lu, C. H.; Guo, X. C.; Chen, F. R.; Yang, H. H.; Wang, X. R. Mussel-Inspired Molecularly Imprinted Polymer Coating Superparamagnetic Nanoparticles for Protein Recognition. *J. Mater. Chem.* **2009**, *20*, 880–883.
35. Zhang, M.; He, X.; Chen, L.; Zhang, Y. Preparation of IDA-Cu Functionalized Core-Satellite Fe3O4/Polydopamine/Au Magnetic Manocomposites and Their Application for Depletion of Abundant Protein in Bovine Blood. *J. Mater. Chem.* **2010**, *20*, 10696–10704.
36. Hong, S.; Kim, K. Y.; Wook, H. J.; Park, S. Y.; Lee, K. D.; Lee, D. Y.; Lee, H. Attenuation of the *in Vivo* Toxicity of Biomaterials by Polydopamine Surface Modification. *Nanomedicine* **2011**, *6*, 793–801.
37. Kang, S. M.; Park, S.; Kim, D.; Park, S. Y.; Ruoff, R. S.; Lee, H. Simultaneous Reduction and Surface Functionalization of Graphene Oxide by Mussel-Inspired Chemistry. *Adv. Funct. Mater.* **2011**, *21*, 108–112.
38. Si, J.; Yang, H. Preparation and Characterization of Bio-Compatible Fe_3O_4@Polydopamine Spheres with Core/Shell Nanostructure. *Mater. Chem. Phys.* **2011**, *128*, 519–524.
39. Chen, T.; Shao, M.; Xu, H.; Zhuo, S.; Liu, S.; Lee, S. T. Molecularly Imprinted Polymer-Coated Silicon Nanowires for Protein Specific Recognition and Fast Separation. *J. Mater. Chem.* **2012**, *22*, 3990–3996.
40. Mrówczyński, R.; Turcu, R.; Leostean, C.; Scheidt, H. A.; Liebscher, J. New Versatile Polydopamine Coated Functionalized Magnetic Nanoparticles. *Mater. Chem. Phys.* **2013**, *138*, 295–302.
41. Zhang, M.; Zhang, X.; He, X.; Chen, L.; Zhang, Y. A Self-Assembled Polydopamine Film on the Surface of Magnetic Nanoparticles for Specific Capture of Protein. *Nanoscale* **2012**, *4*, 3141–3147.
42. Gullotti, E.; Park, J.; Yeo, Y. Polydopamine-Based Surface Modification for the Development of Peritumorally Activatable Nanoparticles. *Pharm. Res.* **2013**, 1–12.
43. Zhang, L.; Wu, J.; Wang, Y.; Long, Y.; Zhao, N.; Xu, J. Combination of Bioinspiration: A General Route to Superhydrophobic Particles. *J. Am. Chem. Soc.* **2012**, *134*, 9879–9881.
44. Yan, J.; Yang, L.; Lin, M. F.; Ma, J.; Lu, X.; Lee, P. S. Polydopamine Spheres as Active Templates for Convenient Synthesis of Various Nanostructures. *Small* **2013**, *9*, 596–603.
45. Ju, K. Y.; Lee, Y.; Lee, S.; Park, S. B.; Lee, J. K. Bioinspired Polymerization of Dopamine to Generate Melanin-Like Nanoparticles Having an Excellent Free-Radical-Scavenging Property. *Biomacromolecules* **2011**, *12*, 625–632.
46. Black, K. C.; Yi, J.; Rivera, J. G.; Zelasko-Leon, D. C.; Messersmith, P. B.Polydopamine-Enabled Surface Functionalization of Gold Nanorods for Cancer Cell-Targeted Imaging and Photothermal Therapy. *Nanomedicine* **2013**, *8*, 17–28.
47. Postma, A.; Yan, Y.; Wang, Y.; Zelikin, A. N.; Tjipto, E.; Caruso, F. Self-Polymerization of Dopamine as a Versatile and Robust Technique to Prepare Polymer Capsules. *Chem. Mater.* **2009**, *21*, 3042–3044.
48. Yu, B.; Wang, D. A.; Ye, Q.; Zhou, F.; Liu, W. Robust Polydopamine Nano/Microcapsules and Their Loading and Release Behavior. *Chem. Commun.* **2009**, 6789–6791.
49. Ochs, C. J.; Hong, T.; Such, G. K.; Cui, J.; Postma, A.; Caruso, F. Dopamine-Mediated Continuous Assembly of Biodegradable Capsules. *Chem. Mater.* **2011**, *23*, 3141–3143.
50. Cui, J.; Yan, Y.; Such, G. K.; Liang, K.; Ochs, C. J.; Postma, A.; Caruso, F. Immobilization and Intracellular Delivery of an Anticancer Drug Using Mussel-Inspired Polydopamine Capsules. *Biomacromolecules* **2012**, *13*, 2225–2228.
51. Cui, J.; Wang, Y.; Postma, A.; Hao, J.; Hosta-Rigau, L.; Caruso, F. Monodisperse Polymer Capsules: Tailoring Size, Shell Thickness, and Hydrophobic Cargo Loading *via* Emulsion Templating. *Adv. Funct. Mater.* **2010**, *20*, 1625–1631.
52. Van der Westen, R.; Hosta-Rigau, L.; Sutherland, D. S.; Goldie, K. N.; Albericio, F.; Postma, A.; Städler, B. Myoblast Cell Interaction with Polydopamine Coated Liposomes. *Biointerphases* **2012**, *7*, 1–9.
53. Bettinger, C. J.; Bruggeman, J. P.; Misra, A.; Borenstein, J. T.; Langer, R. Biocompatibility of Biodegradable Semiconducting Melanin Films for Nerve Tissue Engineering. *Biomaterials* **2009**, *30*, 3050–3057.
54. Tsai, W.-B.; Chen, W.-T.; Chien, H.-W.; Kuo, W.-H.; Wang, M.-J. Poly(Dopamine) Coating of Scaffolds for Articular Cartilage Tissue Engineering. *Acta Biomater.* **2011**, *7*, 4187–4194.
55. Wu, C.; Fan, W.; Chang, J.; Xiao, Y. Mussel-Inspired Porous SiO2 Scaffolds with Improved Mineralization and Cytocompatibility for Drug Delivery and Bone Tissue Engineering. *J. Mater. Chem.* **2011**, *21*, 18300–18307.
56. Yan, P.; Wang, J.; Wang, L.; Liu, B.; Lei, Z.; Yang, S. The *in Vitro* Biomineralization and Cytocompatibility of Polydopamine Coated Carbon Nanotubes. *Appl. Surf. Sci.* **2011**, *257*, 4849–4855.
57. Lynge, M. E.; Ogaki, R.; Laursen, A. O. r.; Lovmand, J.; Sutherland, D. S.; Städler, B. Polydopamine/Liposome Coatings and Their Interaction with Myoblast Cells. *ACS Appl. Mater. Interfaces* **2011**, *3*, 2142–2147.
58. Hosta-Rigau, L.; Jensen, B. E.; Fjeldsø, K. S.; Postma, A.; Li, G.; Goldie, K. N.; Albericio, F.; Zelikin, A. N.; Städler, B. Surface-Adhered Composite Poly(Vinyl Alcohol) Physical Hydrogels: Polymersome-Aided Delivery of Therapeutic Small Molecules. *Adv. Healthcare Mater.* **2012**, *1*, 791–795.
59. Liu, Y.; Ai, K.; Liu, J.; Deng, M.; He, Y.; Lu, L. Dopamine-Melanin Colloidal Nanospheres: An Efficient Near-Infrared Photothermal Therapeutic Agent for *in Vivo* Cancer Therapy. *Adv. Mater.* **2013**, *25*, 1353–1359.
60. Della Vecchia, N. F.; Avolio, R.; Alfè, M.; Errico, M. E.; Napolitano, A.; d'Ischia, M. Building-Block Diversity in Polydopamine Underpins a Multifunctional Eumelanin-Type Platform Tunable Through a Quinone Control Point. *Adv. Funct. Mater.* **2013**, *23*, 1331–1340.
61. Liu, X.; Chen, Y.; Li, H.; Huang, N.; Jin, Q.; Ren, K.; Ji, J. Enhance Retention and Cellular Uptake of Nanoparticles in Tumor by Controlling Their Aggregation Behavior. *ACS Nano* **2013**, *7*, 6244–6257.
62. Lesniak, A.; Fenaroli, F.; Monopoli, M. P.; Åberg, C.; Dawson, K. A.; Salvati, A. Effects of the Presence or Absence of a Protein Corona on Silica Nanoparticle Uptake and Impact on Cells. *ACS Nano* **2012**, *6*, 5845–5857.
63. Liu, X.; Huang, N.; Li, H.; Jin, Q.; Ji, J. Surface and Size Effects on Cell Interaction of Gold Nanoparticles with Both Phagocytic and Non-Phagocytic Cells. *Langmuir* **2013**, *29*, 9138–9148.
64. Cho, E. C.; Zhang, Q.; Xia, Y. The Effect of Sedimentation and Diffusion on Cellular Uptake of Gold Nanoparticles. *Nat. Nanotechnol.* **2011**, *6*, 385–391.
65. Schrand, A. M.; Schlager, J. J.; Dai, L.; Hussain, S. M. Preparation of Cells for Assessing Ultrastructural Localization of Nanoparticles with Transmission Electron Microscopy. *Nat. Protoc.* **2010**, *5*, 744–757.
66. Nativo, P.; Prior, I. A.; Brust, M. Uptake and Intracellular Fate of Surface-Modified Gold Nanoparticles. *ACS Nano* **2008**, *2*, 1639–1644.

67. Park, T. G.; Jeong, J. H.; Kim, S. W. Current Status of Polymeric Gene Delivery Systems. *Adv. Drug Delivery Rev.* **2006**, *58*, 467–486.
68. Li, S.-D.; Huang, L. Pharmacokinetics and Biodistribution of Nanoparticles. *Mol. Pharmaceutics* **2008**, *5*, 496–504.
69. Shah, N. B.; Vercellotti, G. M.; White, J. G.; Fegan, A.; Wagner, C. R.; Bischof, J. C. Blood-Nanoparticle Interactions and in Vivo Biodistribution: Impact of Surface PEG and Ligand Properties. *Mol. Pharmaceutics* **2012**, *9*, 2146–2155.
70. Klippstein, R.; Pozo, D. Nanotechnology-Based Manipulation of Dendritic Cells for Enhanced Immunotherapy Strategies. *Nanomed. Nanotechnol. Biol. Med.* **2010**, *6*, 523–529.
71. Lin, A. Y.; Almeida, J. P. M.; Bear, A.; Liu, N.; Luo, L.; Foster, A. E.; Drezek, R. A. Gold Nanoparticle Delivery of Modified CpG Stimulates Macrophages and Inhibits Tumor Growth for Enhanced Immunotherapy. *PLoS One* **2013**, *8*, e63550.
72. Asanuma, M.; Miyazaki, I.; Ogawa, N. Dopamine-or L-DOPA-Induced Neurotoxicity: the Role of Dopamine Quinone Formation and Tyrosinase in a Model of Parkinson's Disease. *Neurotoxic. Res.* **2003**, *5*, 165–176.
73. Chu, C. Y.; Liu, Y. L.; Chiu, H. C.; Jee, S. H. Dopamine-Induced Apoptosis in Human Melanocytes Involves Generation of Reactive Oxygen Species. *Br. J. Dermatol.* **2006**, *154*, 1071–1079.
74. Zhang, X.; Wang, S.; Xu, L.; Feng, L.; Ji, Y.; Tao, L.; Li, S.; Wei, Y. Biocompatible Polydopamine Fluorescent Organic Nanoparticles: Facile Preparation and Cell Imaging. *Nanoscale* **2012**, *4*, 5581–5584.
75. Grabar, K. C.; Freeman, R. G.; Hommer, M. B.; Natan, M. J. Preparation and Characterization of Au Colloid Monolayers. *Anal. Chem.* **1995**, *67*, 735–743.